Scripta Materialia 154 (2018) 220–224

Contents lists available at ScienceDirect

Scripta Materialia

journal homepage: www.elsevier.com/locate/scriptamat

Regular article

Investigation of a nano-scale, incommensurate, modulated domain in a Ti-Fe alloy

Yufeng Zheng [a,*], Daniel Huber [b], Hamish L. Fraser [a]

[a] Center for the Accelerated Maturation of Materials, Department of Materials Science and Engineering, The Ohio State University, 1305 Kinnear Road, Columbus, OH 43212, USA
[b] Center for Electron Microscopy and Analysis, The Ohio State University, 1305 Kinnear Road, Columbus, OH 43212, USA

ARTICLE INFO

Article history:
Received 5 April 2018
Received in revised form 12 May 2018
Accepted 5 June 2018
Available online xxxx

Keywords:
Titanium alloys
Phase transformations
Incommensurate modulated domain
Scanning transmission electron microscopy
Ti-Fe alloy

ABSTRACT

The microstructure of a Ti-Fe compositional gradient sample was investigated using transmission electron microscopy (TEM) and high angle annular dark field scanning transmission electron microscopy (HAADF-STEM). Different combinations of phases were observed to form depending on the local concentration of Fe. Interestingly, a nano-scale incommensurate modulated domain was detected in the alloy containing approximately 13.8 to 33.9 wt% Fe using selected area diffraction (SAD). The observed disordered structure with no fixed long range periodicity in the nano-scale incommensurate modulated domain in aberration-corrected HAADF-STEM imaging was found not related to the shuffle mechanism of the ω phase.

Microstructural evolution in titanium alloys can be significantly influenced by the nano-scale non-uniformity of alloy composition and/or instability of microstructure during thermal/mechanical processing, and so these may ultimately determine the performance of titanium alloys [1]. Recent studies have revealed several such nano-scale instabilities in a variety of titanium alloys. Thus, in a gum-type metal, Ti-23Nb-0.7Ta-2Zr-1.2O, the Elinvar effect and low modulus are reported to arise from the formation of nano-sized martensite domains [2]. It has been claimed that these domains share the same *orthorhombic* structure of conventional martensite, but are restricted to nano-size scales due to local stress fields produced by defects in the alloy such as impurities and dislocations via a strain glass transition [3, 4]. In another gum-type titanium alloy, Ti-24Nb-4Zr-8Sn, it has been proposed that the combination of high strength and low modulus across a wide temperature range is due to an elastically confined martensitic transformation mechanism [5–7]. Thus, nano-scale regions which are either lean or rich in Nb, as detected by atom probe tomography, are formed above the martensite start temperature by spinodal decomposition and such nano-scale compositional instabilities may confine the subsequent martensite transformation [5, 6]. It has also been reported that, in oxygen-added Ti-Nb based alloys, superelasticity and the temperature dependent shape memory effect are due to the reversible transformation between the nano-sized modulated domains and long range α″ martensite [8, 9]. The origin of such nano-sized modulated domains is proposed to be the local strain caused by the randomly distributed interstitial oxygen atoms in the parent β phase matrix [8–10]. In a recent study by the present authors, two other types of novel nano-scale *orthorhombic* structural instabilities have been found in titanium alloys, named the O′ phase [11–13] and O″ phase [14]. O′ phase is an intrinsic nano-scale structural instability in the parent *bcc* structure phase matrix formed by a shuffle of atomic columns corresponding to the $\{110\}\langle 1\bar{1}0\rangle$ soft-phonon, providing that the amount of solute exceeds a critical value [11–13]. O″ phase is a nano-scale ordered *orthorhombic* structure formed by the ordering of every three {110} planes along the normal <110> direction in an aged Ti-5Al-5Mo-5V-3Cr alloy [14].

In addition to the nano-scale instabilities in titanium alloys described above, there is the well established ω phase that may occur in many titanium alloys and influence subsequent phase transformations. In isomorphous titanium alloys, such as the binaries Ti-Mo and Ti-V, it has been shown that the formation of nano-scale instabilities is also closely related to alloy concentration [11, 15]. For example, full collapse of the $\{111\}_\beta$ planes is characterized in athermal ω phase in as-quenched Ti-12wt%Mo, whereas only partial collapse of these planes occurs in athermal ω in as-quenched Ti-18wt%Mo; in those latter alloy, partially-collapsed ω coexists with the *orthorhombic* O′ phase [11]. The partial collapse is due to the increased amount of Mo which impedes the atomic collapse along the $\langle 111\rangle_\beta$ direction because of bond strength differences [15] and activation of the $\{110\}\langle 1\bar{1}0\rangle$ soft-phonon [11]. In contrast, in an eutectoid type titanium alloy, i.e., Ti-Fe,

* Corresponding author at: CAMM, The Ohio State University, 1305 Kinnear Rd., Suite 100, Columbus, OH 43212-1177, USA.
E-mail address: zheng.510@osu.edu (Y. Zheng).

https://doi.org/10.1016/j.scriptamat.2018.06.010
1359-6462/

Ti-Mn and Ti-Fe-Mo alloys, it has been reported that metastable athermal ω phase and an incommensurate ω phase form depending on the concentration of the solute content [16–18], and that in the incommensurate ω phase, atoms shuffle towards each other but do not form the correct periodic pattern, i.e. in the alloy of Ti-22at%Fe (≈Ti-24.8wt%Fe) [16]. However, this very interesting observation of an incommensurate phase has been made without the provision of detailed experimental data showing the actual structure, a task that would require direct atomic imaging using a technique such as aberration-corrected HAADF-STEM. Hence, the structure of the incommensurate phase has not been determined rigorously in the eutectoid type titanium alloy containing high concentration of β phase stabilizers, and actually remains an open question. In the present study, this question is addressed by use of a compositionally graded Ti-Fe sample, permitting a systematic study of the nano-scale incommensurate modulated domains in the concentration range from approximately Ti-13.8wt%Fe to Ti-33.9wt%Fe using TEM and HAADF-STEM imaging, and making a comparison with the athermal ω phase in Ti-4.8wt%Fe.

The Ti-Fe compositional gradient button was partially arc melted in a high-purity Ar atmosphere on a water cooled copper hearth. The pure Fe (purity > 99.9%) was placed on top of a 7 mm thick pure Ti plate (purity > 99.9%) and rapidly heated by the arc, that partially melted the Fe and Ti plate producing a steep compositional gradient at the Fe/Ti interface. The sample for analysis was cut at the region containing such compositional gradient in the as-melted button and prepared using conventional grinding and polishing. The microstructure in the polished sample was characterized in an FEI Sirion FEG scanning electron microscope (SEM) operating at 12 kV and the compositional gradient in the polished sample was assessed using X-ray energy dispersive spectroscopy (XEDS) in the same SEM operating at 20 kV. TEM foils were prepared from three specific sites in the sample containing various amounts of Fe using Focused Ion Beam (FIB) techniques, employing an FEI Helios Nanolab 600 system. The lift-out samples were cleaned with Ar^+ ions at low voltages using a Fischione Model 1040 Nanomill. TEM SAD and dark-field images were collected on a Philips CM200 TEM at 200 kV and HAADF-STEM images were recorded using a probe-corrected FEI Titan3™ 80-300 operating with an accelerating voltage of 300 kV. STEM XEDS analysis was conducted using an image-corrected Titan3™ G2 60-300 (S)TEM equipped with FEIs ChemiSTEM XEDS technology.

In order to explore the distribution of Fe qualitatively and locate the sites for TEM analysis, the composition of the section of the partially arc-melted sample was analyzed using SEM XEDS. It was found that the composition varied from approximately 5 wt% to 35 wt% Fe. The microstructure of the sample is shown in Fig. 1(a); the lower and upper parts of the image correspond to the low (5 wt%, shown in STEM XEDS mapping in Fig. 1(b)) and high Fe (35 wt%) concentrations, respectively. Three distinct microstructural features may be seen in the backscattered SEM image. Thus, in the Fe lean region, the microstructure consists of a coarse plate morphology with irregularly shaped interfaces, whereas in the Fe rich region, an eutectic-type lamellar microstructure is observed. In the ~30 μm wide region in between, there are a small number of coarse grains without any visible precipitates. As shown in Fig. 1(a), TEM foils were prepared using FIB techniques for subsequent analysis from three specific sites, marked as 1, 2, and 3 in the figure.

The microstructures in the three thin foils, taken, as noted above, from the sites marked 1, 2, and 3, have been characterized. Thus, the SAD patterns obtained from these three sites, in each case with the electron beam being parallel to $[110]_\beta$ zone axis, are shown in Fig. 2(a–c). The average composition of the first foil (site 1) was determined to be Ti-4.8wt%Fe. Strong reflections near 1/2 $\{112\}_\beta$ indicating the presence of the *hcp* α phase, highlighted using red circles, are observed in Fig. 2(a), as well as extra reflections at 1/3 and 2/3 $\{112\}_\beta$ indicating the presence of the *hexagonal* ω phase, highlighted using yellow circles. It appears then that the precipitates, with the coarse plate morphology and irregular interfaces, are the α phase. Because Fe is a very strong β phase stabilizer, the α precipitates contain high concentrations of Ti but low amounts of Fe and athermal ω phase is formed in the β phase region with the average concentration of 8.2 wt% Fe, as measured in STEM XEDS shown in Fig. 1(b).

The second thin foil was taken from site 2 (Fig. 1(a)), located near the center of the coarse grain shown in Fig. 1(a), and its measured average composition is Ti-13.8wt%Fe. In the $[110]_\beta$ zone axis diffraction pattern (Fig. 2(b)), additional reflections are observed and these are highlighted by the yellow circles. Compared with ω phase reflections shown in Fig. 2(a), these additional reflections shift from the 1/3 and 2/3 $\{112\}_\beta$ sites, and are elongated into a rod-like shapes and become more smeared and diffuse. This is consistent with the reported diffraction pattern obtained from the incommensurate ω phase [16–18]. A dark field image formed by selecting the highlighted four reflections (Fig. 2(b)) is shown in Fig. 2(d), and nano-scale domains can be observed randomly distributed in parent β phase matrix. The size and distribution of these domains are similar to that of incommensurate ω particles shown in [17]. Therefore, the nano-scale domains observed in Fig. 2(b) and Fig. 2(d) from the Ti-13.8wt%Fe are believed to be the same particles as were claimed to be incommensurate ω phase in the literature [16–18].

The measured average composition of the third foil (site 3, Fig. 1(a)) prepared near the eutectic lamellar microstructure is Ti-33.9wt%Fe. In Fig. 2(c), superlattice reflections are observed at 1/2 $\{002\}_\beta$ highlighted by green circles, and these are consistent with the expected presence of a B2 (TiFe) phase, with an orientation relationship between the ordered B2 phase and β matrix given by $\{001\}_{B2}//\{001\}_\beta$ and $<110>_{B2}//<110>_\beta$. XEDS maps and line profile shown in Fig. 3(a–c) are consistent with the two phases being β-Ti (high Ti, and low Fe contents) and the B2 phase (very close to being equiatomic in concentration, as expected from the stoichiometry of this phase). Interestingly, in Fig. 2(c), it is noticed that the highlighted additional reflections (using yellow circles) shift further away from those expected of the ω phase and still exhibit a diffuse rod-like shape. When combining the diffraction information

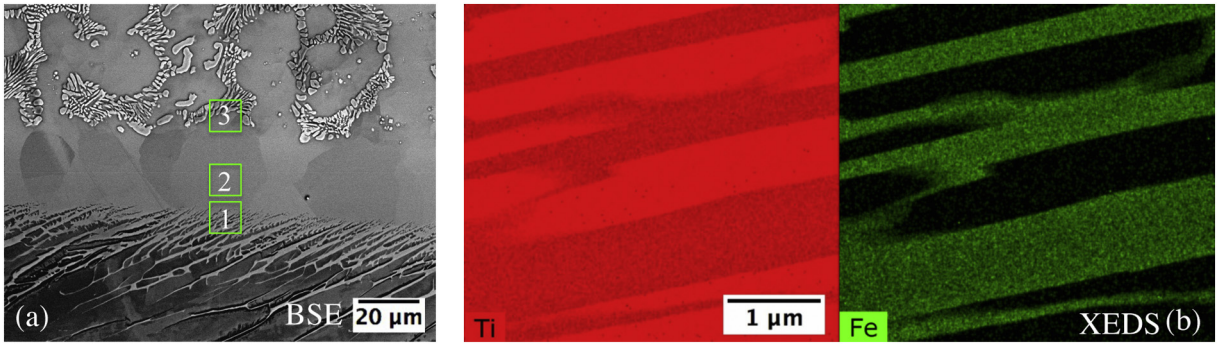

Fig. 1. (a) Backscattered SEM image showing the microstructure of the partially arc-melted Ti-Fe compositional gradient sample; (b) STEM XEDS mapping of Ti and Fe showing the Fe lean coarse plate morphology microstructure.